On Some High Resolution Schemes for Stably Stratified Fluid Flows

Tomáš Bodnár and Luděk Beneš

Abstract The aim of this paper is to present some high-resolution numerical methods in the context of the solution of stably stratified flow of incompressible fluid. Two different numerical methods are applied to a simple 2D test case of wall bounded flow and results are compared and discussed in detail with emphasize on the specific features of stratified flows. The two numerical methods are the AUSM finite–volume scheme and the high order compact finite-difference scheme.

Keywords finite–volume, finite–difference, stratification, compact, AUSM
MSC2010: 65M08, 65M06, 76D05, 76D50, 76D33

1 Introduction

The numerical solution of stably stratified fluid flows represents a challenging class of problems in modern CFD. This study was motivated by the air flow in the stably stratified Atmospheric Boundary Layer, where the presence of stratification leads to appearance of gravity waves in the proximity of terrain obstacles. These small–amplitude waves are affecting the flow–field at large distances which is in contrast to the typical non-stratified case, where the flow–field is only affected locally in the close proximity of the obstacle. The wavelength of these waves is governed by the Brunt–Väisälä frequency, i.e depends on the product of the gravity acceleration and the background density gradient.

Tomáš Bodnár
Institute of Thermomechanics, Academy of Sciences of Czech Republic, Dolejškova 5, 182 00 Prague 8, Czech Republic, e-mail: bodnar@marian.fsik.cvut.cz

Luděk Beneš
Department of Tech. Mathematics, Faculty of Mech. Engineering, Czech Technical University in Prague, Karlovo Náměstí13, 121 35 Prague 2 Czech Republic, e-mail: Ludek.Benes@fs.cvut.cz

J. Fořt et al. (eds.), *Finite Volumes for Complex Applications VI – Problems & Perspectives*, Springer Proceedings in Mathematics 4,
DOI 10.1007/978-3-642-20671-9_16,

From the numerical point of view, the simulations of stratified fluid flows are in general more demanding than the solution of similar non-stratified flow cases (see our previous work [10], [4], [1], or [6]). First of all the *model of stratified fluid flow* has to be chosen. Such models are based on variable-density incompressible fluid model including gravity force terms. A simple approximation of such model is developed in Sect. 2. The appearance of the gravity waves in the computational field adds some more constrains on the choice of *numerical scheme and grid*. The limiting factor here is the proper resolution of gravity waves in the whole domain with sufficient number of grid points per wavelength and low amount of numerical dumping to preserve the resolved gravity waves rather than excessively dumping them. Last but not least problem comes with *boundary conditions*. Their proper choice and implementation affects the computational field much strongly than in the non–stratified case.

One of the aims of this paper is to demonstrate that the high-order compact finite-difference schemes offer an interesting alternative to the modern finite–volume discretizations. Beside of the high resolving capabilities of both methods, the compact discretizations have well defined dispersion/diffusion properties and thus can safely be applied to the numerical simulations of wave phenomena. These specific properties of compact discretizations have been successfully used in computational aeroacoustics. This paper is one of the first attempts to use these wave resolving capabilities in the numerical solution of stratified fluid flows.

2 Mathematical Model

Full incompressible model The motion equations describing the flow of incompressible Newtonian fluid could be written in the following general form

$$\frac{\partial u}{\partial x} + \frac{\partial v}{\partial y} + \frac{\partial w}{\partial z} = 0 \tag{1}$$

$$\frac{\partial \rho}{\partial t} + \frac{\partial (\rho u)}{\partial x} + \frac{\partial (\rho v)}{\partial y} + \frac{\partial (\rho w)}{\partial z} = 0 \tag{2}$$

$$\rho \left(\frac{\partial u}{\partial t} + \frac{\partial (u^2)}{\partial x} + \frac{\partial (uv)}{\partial y} + \frac{\partial (uw)}{\partial z} \right) = -\frac{\partial p}{\partial x} + \mu \Delta u \tag{3}$$

$$\rho \left(\frac{\partial v}{\partial t} + \frac{\partial (uv)}{\partial x} + \frac{\partial (v^2)}{\partial y} + \frac{\partial (vw)}{\partial z} \right) = -\frac{\partial p}{\partial y} + \mu \Delta v \tag{4}$$

$$\rho \left(\frac{\partial w}{\partial t} + \frac{\partial (uw)}{\partial x} + \frac{\partial (vw)}{\partial y} + \frac{\partial (w^2)}{\partial z} \right) = -\frac{\partial p}{\partial z} + \mu \Delta w + \rho g \tag{5}$$

The governing system (1)–(5) for unknowns $\boldsymbol{u}$, p and ρ is sometimes called the Non-homogeneous (incompressible) Navier-Stokes equations.

The small perturbation approximation Now we will assume that the pressure and density fields are perturbation of hydrostatic equilibrium state, i.e.:

$$\rho(x, y, z, t) = \rho_0(z) + \rho'(x, y, z, t) \tag{6}$$

$$p(x, y, z, t) = p_0(z) + p'(x, y, z, t) \tag{7}$$

where the background density and pressure fields are linked by the hydrostatic relation:

$$\frac{\partial p_0}{\partial z} = \rho_0 g. \tag{8}$$

The small perturbation approximation of momentum equations is obtained by introducing the above decomposition of density and pressure into the momentum equations (3), (4) and (5). The density perturbation ρ' is neglected on the left–hand side while on the right–hand side it is retained. On the right–hand side we have removed the hydrostatic pressure using the relation (8) and the fact that according to (7) the horizontal parts of the background pressure gradient are zero.

$$\frac{\partial u}{\partial x} + \frac{\partial v}{\partial y} + \frac{\partial w}{\partial z} = 0 \tag{9}$$

$$\frac{\partial \rho'}{\partial t} + \frac{\partial(\rho' u)}{\partial x} + \frac{\partial(\rho' v)}{\partial y} + \frac{\partial(\rho' w)}{\partial z} = -w\frac{\partial \rho_0}{\partial z} \tag{10}$$

$$\frac{\partial u}{\partial t} + \frac{\partial(u^2)}{\partial x} + \frac{\partial(uv)}{\partial y} + \frac{\partial(uw)}{\partial z} = \frac{1}{\rho_0}\left(-\frac{\partial p'}{\partial x} + \mu \Delta u\right) \tag{11}$$

$$\frac{\partial v}{\partial t} + \frac{\partial(uv)}{\partial x} + \frac{\partial(v^2)}{\partial y} + \frac{\partial(vw)}{\partial z} = \frac{1}{\rho_0}\left(-\frac{\partial p'}{\partial y} + \mu \Delta v\right) \tag{12}$$

$$\frac{\partial w}{\partial t} + \frac{\partial(uw)}{\partial x} + \frac{\partial(vw)}{\partial y} + \frac{\partial(w^2)}{\partial z} = \frac{1}{\rho_0}\left(-\frac{\partial p'}{\partial z} + \mu \Delta w + \rho' g\right) \tag{13}$$

This model is in 2D (x–z) version used for all the simulations presented in this work.

3 Numerical Methods

Two different numerical methods were chosen to perform a comparative study allowing for cross-comparison of results. The first method is the AUSM finite–volume scheme. For comparison, the compact finite–difference schemes were implemented.

3.1 AUSM Finite–Volume Scheme

This method has been chosen to represent the modern high resolution finite–volume schemes. This particular scheme was previously used for the simulation of stratified flow and compared successfully with other methods in [2], [3].

Space discretizations For numerical solution the artificial compressibility method in dual time was used. Continuity equation is rewritten in the form (in 2D, x–z plane)

$$\frac{\partial p}{\partial \tau} + \beta^2 (\frac{\partial u}{\partial x} + \frac{\partial w}{\partial z}) = 0$$

where τ is the artificial time. The equations (9)–(13) rewritten in the 2D conservative form are

$$P W_t + F(W)_x + G(W)_y = S(W).$$

Here $W = [\rho', u, v, p]^T$, $F = F^i - \nu F^v$ and $G = G^i - \nu G^v$ contain the inviscid fluxes F^i, G^i and viscous fluxes F^v and G^v, S is the source term, and $P = diag(1, 1, 1, 0)$. the fluxes and the source term are

$$F^i(W) = [\rho' u, u^2 + p, uw, \beta^2 u]^T, \qquad G^i(W) = [\rho' w, uw, w^2 + p, \beta^2 w]^T, \quad (14)$$

$$F^v(W) = [0, u_x, w_x, 0]^T, \quad G^v(W) = [0, u_y, w_y, 0]^T, \quad S(W) = [-w d\rho_0/dz, 0, \rho' g, 0]^T.$$

The finite volume AUSM scheme was used for spatial discretizations of the inviscid fluxes:

$$\int_\Omega (F^i_x + G^i_y) dS = \oint_{\partial\Omega} (F^i n_x + G^i n_y) dl \approx \sum_{k=1}^{4} \left[u_n \begin{pmatrix} \varrho \\ u \\ w \\ \beta^2 \end{pmatrix}_{L/R} + p \begin{pmatrix} 0 \\ n_x \\ n_y \\ 0 \end{pmatrix} \right] \Delta l_k \quad (15)$$

where n is normal vector, u_n is normal velocity vector, and $(q)_{L/R}$ are quantities on left/right hand side of the face respectively. These quantities are computed using MUSCL reconstruction with Hemker–Koren limiter.

$$q_R = q_{i+1} - \frac{1}{2}\delta_R \quad q_L = q_i + \frac{1}{2}\delta_L$$

$$\delta_{L/R} = \frac{a_{L/R}(b^2_{L/R} + 2) + b_{L/R}(2a^2_{L/R} + 1)}{2a^2_{L/R} + 2b^2_{L/R} - a_{L/R} b_{L/R} + 3}$$

$$a_R = q_{i+2} - q_{i+1} \quad a_L = q_{i+1} - q_i \quad b_R = q_{i+1} - q_i \quad b_L = q_i - q_{i-1}$$

The viscous fluxes are discretized in central way on a dual mesh. This scheme is formally of the second order of accuracy in space.

Time integration For the finite–volume AUSM scheme a fully unsteady solver was used. The dual time stepping approach was adopted, so the separate time–discretizations were needed for physical and artificial time. The derivative with respect to the physical time t is discretized by the second order BDF formula,

$$P\frac{3W^{n+1}-4W^{n}+W^{n-1}}{2\Delta t}+F_x^{n+1}(W)+G_y^{n+1}(W)=S^{n+1} \tag{16}$$

$$Rez^{n+1}(W)=P(\frac{3}{2\Delta t}W^{n+1}-\frac{2}{\Delta t}W^{n}+\frac{1}{2\Delta t}W^{n-1})+F_x^{n+1}(W)+G_y^{n+1}(W)-f^{n+1}-S^{n+1}.$$

Arising system of equations is solved by artificial compressibility method in the dual (artificial) time τ by an explicit 3–stage Runge-Kutta method.

3.2 Compact Finite-Difference Schemes

Here again the artificial compressibility method was used. The solver is limited to steady problems solution, employing the time–marching method.

Space discretizations The spatial discretizations used in this work is directly based on the paper [8], where the class of very high order compact finite difference schemes was introduced and analyzed. The main idea used to construct this family of schemes is that instead of approximating the spatial derivatives ϕ' of certain quantity ϕ explicitly from the neighboring values ϕ_i, the (symmetric) linear combination of neighboring derivatives $(\ldots,\phi'_{i-1},\phi'_i,\phi'_{i+1},\ldots)$ is approximated by weighted average of central differences.

The simplest compact finite–difference schemes use the approximation in the form

$$a\,\phi'_{i-1}+\phi'_i+a\,\phi'_{i+1}=\alpha_1\frac{\phi_{i+1}-\phi_{i-1}}{2h}+\alpha_2\frac{\phi_{i+2}-\phi_{i-2}}{4h} \tag{17}$$

Here $h=x_i-x_{i-1}$ is the spatial step, while a and α_k are the coefficients determining the specific scheme within the family described by (17). It is easy to see that e.g. for $a=0$, $\alpha_1=1$ and $\alpha_2=0$, the explicit second order central discretizations is recovered. For the simulations presented here, the following coefficients were used:

$$\alpha_1=\frac{2}{3}(a+2)\qquad\qquad \alpha_2=\frac{1}{3}(4a-1). \tag{18}$$

This choice of parameters leads to a one–parametric family of formally fourth order accurate schemes. For $a=0$ the classical explicit fourth order discretizations is recovered, while for $a=0.25$ the well known Padé scheme is obtained.

The above presented schemes are based on central discretizations in space and thus non-physical oscillations can occur in the numerical approximations. A very efficient algorithm for filtering out these high frequency oscillations was proposed

in [8]. The low–pass filter (for the filtered values $\widehat{\phi}_i$) can be formulated in a form very similar to (17):

$$b\,\widehat{\phi}_{i-1} + \widehat{\phi}_i + b\,\widehat{\phi}_{i+1} = 2\beta_0\phi_i + \beta_1\frac{\phi_{i+1}+\phi_{i-1}}{2h} + \beta_2\frac{\phi_{i+2}+\phi_{i-2}}{4h} + \dots \quad (19)$$

The filters of different orders could be obtained for various choices of coefficients. Here the sixth order filter with coefficients

$$\beta_0 = \frac{1}{16}(11{+}10b);\ \beta_1 = \frac{1}{32}(15{+}34b);\ \beta_2 = \frac{1}{16}(6b{-}3);\ \beta_3 = \frac{1}{32}(1{-}2b) \quad (20)$$

was used. For other filters see e.g. [12]. The parameter $-0.5 < b < 0.5$ is used to fine–tune the filter.[1] More information on the compact space discretizations can be found in [8], [12], [7].

Temporal discretizations The system of governing Partial Differential Equations was discretized in space using the above described finite–difference technique. This leads to a system of Ordinary Differential Equations for time-evolution of grid values of the vector of unknowns W. Resulting system of ODE's can be solved by a suitable time-integration method. In this study we have used the so called Strong Stability Preserving Runge–Kutta methods [9,11]. The three stage second order SSP Runge–Kutta method was used to obtain the results presented here.

4 Numerical Results

Computational domain The 2D computational domain is selected as a part of wall-bounded half space with low smooth cosine-shaped hill. The hill height is $h = 1m$, while the whole domain has dimensions $90 \times 30\,m$. The numerical simulations were performed on a structured, non-orthogonal wall-fitted grid that has 233×117 points with the minimum cell size in the near-wall region $\Delta z = 0.03m$. The grid is smoothly coarsened from the proximity of the hill towards the far field. The maximum growth of consequent cells is 3%.

Boundary conditions On the *inlet* the velocity profile $\boldsymbol{u} = (u(z), 0, 0)$ is prescribed. The horizontal velocity component u is given by $u(z) = U_0(z/H)^{1/r}$ with $U_0 = 1m/s$ and $r = 40$. Density perturbation ρ' is set to zero, while homogeneous Neumann condition is used for pressure. On the *outlet* the homogeneous Neumann condition is prescribed for all velocity components, as well as for the density perturbations. Pressure is set to a constant. On the *wall* the no-slip conditions are

[1] In order to distinguish between different finite–difference schemes we use the notation $CX_{aaa}FY_{bbb}$ for compact scheme of order X with parameter $a =$ aaa combined with filter of order Y applied with the dumping parameter $b =$ bbb.

used for velocity. Homogeneous Neumann condition is used for pressure and density perturbation. For *free stream* the homogeneous Neumann condition is used for all quantities including pressure and density perturbations.

The background density field is given by $\rho_0(z) = \rho_w + \gamma z$ with $\rho_w = 1.2\,kg \cdot m^{-3}$ and $\gamma = -0.01\,kg \cdot m^{-4}$. The gravity acceleration was set to $g = -50\,m \cdot s^{-2}$ to test the behavior of the model and numerical method for sufficiently high Brunt–Väisälä frequency (i.e. short wavelength). The Reynolds number was in the range 100–500 (i.e. $\mu = 1 \cdot 10^{-2} - 2 \cdot 10^{-3} kg \cdot m^{-1} \cdot s^{-1}$).

Numerical results The small hill placed at the origin of the coordinate system generates a perturbation in the density field. Due to the buoyancy term in the equation (13), this density perturbation is translated into vertical motion that is superposed to the mean horizontal flow. The gravity waves are best visible in the vertical velocity contours (Fig. 1–4). The same color scale was used in all figures. The results of both schemes are quite close to each other as it is visible from the

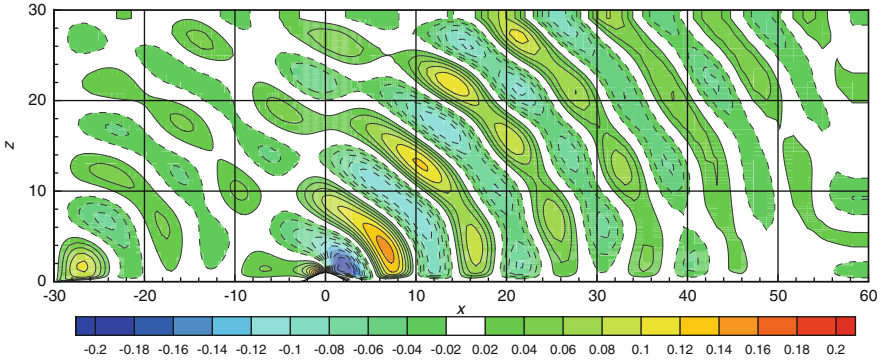

Fig. 1 Vertical velocity contours - $Re = 500$ - Compact scheme $C4_{038}F6_{049}$

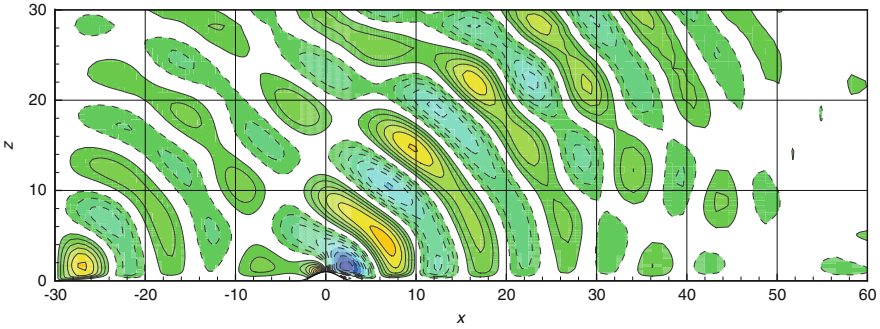

Fig. 2 Vertical velocity contours - $Re = 500$ - AUSM scheme

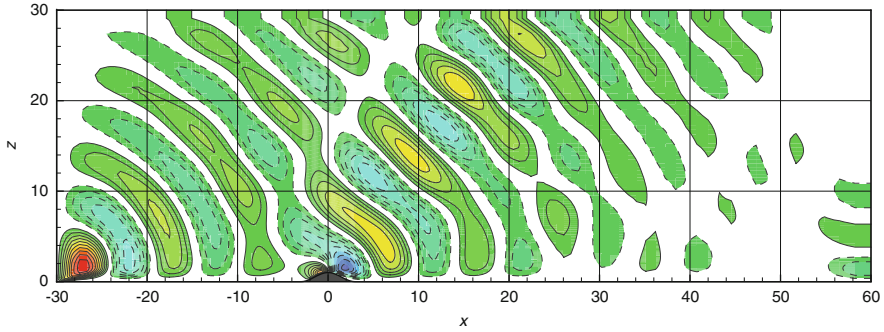

Fig. 3 Vertical velocity contours - $Re = 100$ - Compact scheme $C4_{038}F6_{049}$

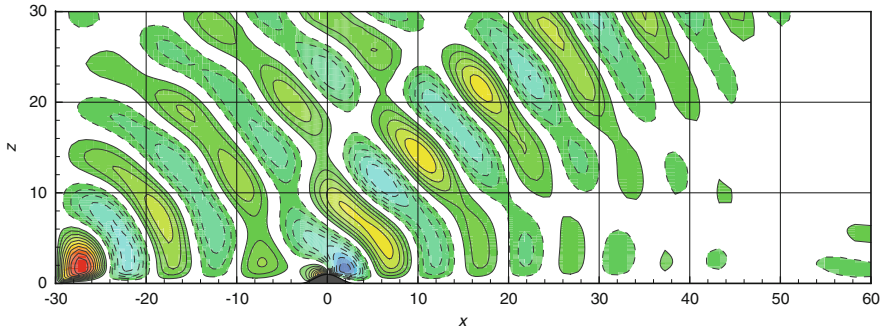

Fig. 4 Vertical velocity contours - $Re = 100$ - AUSM scheme

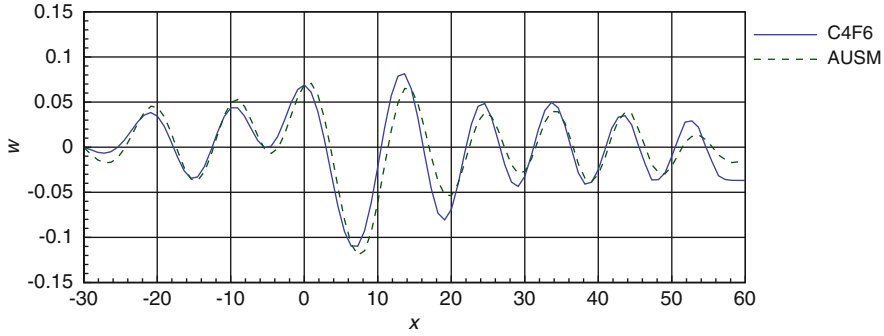

Fig. 5 Vertical velocity profiles comparison for $Re = 500$ in a horizontal cut at the height $z = 10\,m$

vertical velocity profiles shown in the Fig. 5. The basic structure of the results of both numerical methods is very similar. The compact finite difference scheme has clearly an advantage in being able to resolve the gravity waves in the far–field regions where the grid is very coarse.

5 Conclusions and Remarks

The numerical test have demonstrated the ability of both numerical methods to capture the main features of stably stratified flows. The advantage of high order methods was well documented by resolving the gravity waves in the regions of very coarse grid. The numerical simulations have brought some more problems that need to be further explored in detail. From these issues let's mention the the non–physical waves generated and reflected by the artificial boundaries, strong influence of numerical discretization/stabilization techniques on the small amplitude gravity waves, and the grid spacing limits related to Brunt–Väisälä frequency. Some of these problems are discussed in more detail in our recent study [5].

Acknowledgements The financial support for this work was partly provided by the Research Plan *MSM 6840770010* of the Ministry of Education of Czech Republic.

References

1. L. Beneš, T. Bodnár, P. Fraunié, K. Kozel, Numerical modelling of pollution dispersion in 3D atmospheric boundary layer, in: B. Sportisse (Ed.), Air Pollution Modelling and Simulation, Springer Verlag, 2002, pp. 69–78.
2. L. Beneš, J. Fürst, Numerical simulation of stratified flows past a body, in: ENUMATH 2009, Springer, 2009, p. 8p.
3. L. Beneš, J. Fürst, Comparison of the two numerical methods for the stratified flow, in: ICFD 2010 10th Conference on Numerical Methods for Fluid Dynamics, Univ. Reading, 2010, p. 6p.
4. T. Bodnár, L. Beneš, K. Kozel, Numerical simulation of flow over barriers in complex terrain, Il Nuovo Cimento C 31 (5–6) (2008) 619–632.
5. T. Bodnár, L. Beneš, Ph. Fraunié, K. Kozel, Application of Compact Finite-Difference Schemes to Simulations of Stably Stratified Fluid Flows, Preprint submitted to Applied Mathematics and Computation (2011).
6. T. Bodnár, K. Kozel, P. Fraunié, Z. Jaňour, Numerical simulation of flow and pollution dispersion in 3D atmospheric boundary layer, Computing and Visualization in Science 3 (1–2) (2000) 3–8.
7. D. V. Gaitonde, J. S. Shang, J. L. Young, Practical aspects of higher-order numerical schemes for wave propagation phenomena, International Journal for Numerical Methods in Engineering 45 (1999) 1849–1869.
8. S. K. Lele, Compact finite difference schemes with spectral-like resolution, Journal of Computational hysics 103 (1992) 16–42.
9. C. W. Shu, S. Osher, Efficient implementation of essentially non-oscillatory shock-capturing schemes, Journal of Computational Physics 77 (1988) 439–471.
10. I. Sládek, T. Bodnár, K. Kozel, On a numerical study of atmospheric 2D and 3D - flows over a complex topography with forest including pollution dispersion, Journal of Wind Engineering and Industrial Aerodynamics 95 (9–11).
11. R. J. Spiteri, S. J. Ruuth, A new class of optimal high-order strong-stability-preserving time discretization methods, SIAM Journal on Numerical Analysis 40 (2) (2002) 469–491.
12. M. R. Visbal, D. V. Gaitonde, On the use of higher-order finite-difference schemes on curvilinear and deforming meshes, Journal of Computational Physics 181 (2002) 155–185.

The paper is in final form and no similar paper has been or is being submitted elsewhere.